Materials & Design 227 (2023) 111741

Contents lists available at ScienceDirect

Materials & Design

journal homepage: www.elsevier.com/locate/matdes

X-ray computed tomography for predictive quality assessment, 3D visualisation of micro-injection mouldings and soft-tool deformation

Mert Gülçür [a,*], Paul Wilson [a], Michael Donnelly [a], Kevin Couling [a], Vannessa Goodship [a], Jérôme Charmet [b,c], Mark A. Williams [a], Gregory Gibbons [a]

[a] WMG, University of Warwick, UK
[b] WMS, University of Warwick, UK
[c] School of Engineering–HE-Arc Ingénierie, HES-SO University of Applied Sciences Western Switzerland, 2000 Neuchâtel, Switzerland

HIGHLIGHTS

- X-ray computed tomography (XCT) is demonstrated for quality inspection of micro-injection mouldings and soft-tool deformation.
- XCT results compared against laser-scanning confocal microscopy.
- The approach provided an in-line quality predictive model up to 92% accuracy for filling prediction.

GRAPHICAL ABSTRACT

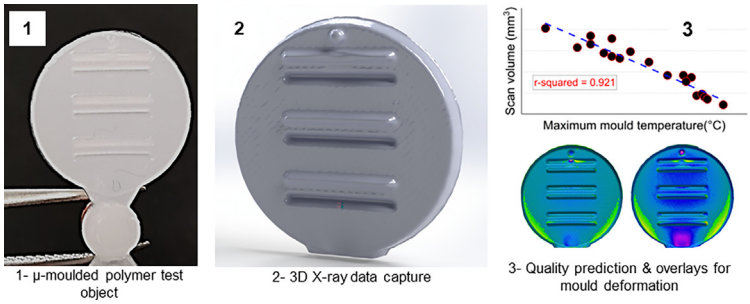

1- µ-moulded polymer test object

2- 3D X-ray data capture

3- Quality prediction & overlays for mould deformation

ARTICLE INFO

Article history:
Received 3 November 2022
Revised 25 January 2023
Accepted 11 February 2023
Available online 20 February 2023

Keywords:
X-ray
X-ray computed tomography
Micro-injection moulding
3D visualisation
Injection moulding
Rapid prototyping
Additive manufacturing

ABSTRACT

This work presents X-ray computed tomography (XCT) as a dimensional quality assurance technique for micro-injection moulded polymeric test objects for the establishment of predictive quality models and quantifying soft-tool deformation. The results are compared against an industry standard laser-scanning-confocal microscope (LSCM) for the evaluation of XCT's capability. The work demonstrates; (i) the exploitation of a XCT equipment for dimensional characterisation of micro-injection moulded products made out of polymers with adequate acquisition times, (ii) that acquired XCT data from the 3D visualisation of the micromouldings perform on par with a laser-scanning-confocal microscope in a quality prediction model, (iii) that the deformation occurring in an additively manufactured soft-tool can be quantified using XCT. The technique was particularly superior in volumetric data acquisition compared to LSCM in the filling prediction of the micromouldings. Better accuracy and repeatability in predicting the quality of the mouldings up to 92% achieved with XCT, in conjunction with an in-line collected soft-tool surface temperature data as an indirect quality assurance method. Given the capability of the XCT for the 3D data acquisition of polymeric miniature components, the approach described here has great potential in high-value micro-manufacturing process quality modelling for in-line quality assessment of miniature and added value products in data-rich contexts.

Rendered 3D animation of the X-ray CT data: https://youtu.be/KwZty_yoDfs.

Abbreviations: XCT, X-ray computed tomography; µ-IM, Micro-injection moulding; LSCM, Laser-scanning confocal microscopy; PP, Polypropylene; T_{max}, Maximum temperature measured on the soft-tool; FDK, Feldkamp, Davis and Kress; H_D, Dome height; L_R, Lowest height of the ridge; V_D, Dome volume; V_T, Total volume; CoV, Coefficient of variation; ε, Relative error; ϑ_o, Observed value; ϑ_e, Expected value; r^2, r-squared or coefficient of determination; STL, Stereolithography or standard triangle language.

* Corresponding author at: WMG, International Manufacturing Centre, University of Warwick, Coventry CV4 7AL, UK.

https://doi.org/10.1016/j.matdes.2023.111741
0264-1275/

1. Introduction

The increasing capability of micro-manufacturing processes enables the manufacture of miniature products with extremely small dimensions, complexity, and net-shape for a wide range of applications [1]. Demanding metrology requirements are present for ensuring that the products with micro and nano features are of sufficient and acceptable quality. Advanced microscopy techniques have already been widely utilised for such purpose, often measuring a single critical characteristic of the products for the development of quality predictive models [2,3]. The capture of 3D topology of the micro-manufactured product is obviously more desirable, providing full visualisation and implementation of data-rich approaches. However, the data-intensive aspect of 3D visualisation makes the methods such as laser-scanning or profilometry cumbersome and impractical for micro-manufacturing applications. On this basis, X-ray computed Tomography (XCT) have unique advantages with the recent advancements in the technology with the material and right acquisition parameter selection to provide 3D data acquisition of the objects at adequate speeds.

The process of XCT is similar to conventional radiography, in which X-rays are emitted from an X-ray source towards the object of interest. These X-rays are attenuated relatively based on the local composition of material through which they travel, denser objects resulting in higher attenuation. The penetrating X-rays are then registered by a photon-sensitive detector panel to create a radiograph. Where XCT differs however is that a series of radiographs are acquired by rotating the object by a small increment and repeating the process until radiographs 360° around the object are acquired. This set of projections are then subjected to reconstruction, most commonly FDK (Feldkamp, Davis and Kress) algorithm [4], which creates a voxelised 3D grid of grey values that represents local relative density at the voxel size of the scan, ranging from < 1 μm to 300 μm depending on hardware and object [5,6].

Although being an extremely powerful technique with many recent developments in commercial systems, XCT is still a developing technology and involves relatively time-intensive workflows for the characterisation of technological components including acquisition time, reconstruction, and post-processing [7–12]. To tackle these challenges, commercial systems now offer significant advantages to reduce the acquisition times to increase throughput and availability of system to more users [11]. Moreover, reconstruction and post-processing steps can be potentially automated for utilising XCT towards quality assessment of high-throughput and high-value products [6].

Generally speaking, acquisition times for XCT data are dominantly governed by exposure time and number of projections needed to be acquired, and both values are contingent on a number of complex, interrelated settings [12,13]. Exposure time describes the duration that the detector is exposed to X-rays to acquire a single projection, with larger and denser objects requiring higher exposure to fully penetrate. In this context, XCT of high-added value prototypes or components made out of soft-materials (polymers) can be scanned significantly quicker with lower exposure times as compared to denser materials, e.g., metals with sufficient spatial resolutions [14,15]. This feature can potentially be exploited for technological products manufactured by polymer replication techniques such as injection moulding, hot embossing, and micro-injection moulding, all of which require extensive quality assurance procedures [16–20]. Micro-injection moulding (μ-IM) in particular is thought to be the manufacturing technique which would benefit most from a quality assessment using XCT since the miniature parts manufactured by μ-IM are products often made from single material or polymers, with very high value margins such as medical devices, intricate microsystem components and optics [19–23]. The combination of XCT with sufficient spatial resolution and automated data processing will provide the opportunity for creating predictive models for quality assurance in micro-manufacturing applications [3,22]. This comes with the advantage of having full 3D visualisation of the product, rather than having only the surface point cloud data of interest which is typically provided by standard metrology techniques such as coherence scanning interferometry, focus variation microscopy and laser-scanning-confocal microscopy (LSCM) [20,23,24]. LSCM stands out amongst them, offering the advantage of laser scanning technology for acquiring 3D topography of the measured surface with minimal material limitations which can be advantageous for polymeric micro-featured products due to their translucent or transparent characteristics [24]. However, even though LSCM has higher spatial resolution than XCT, the technique can only acquire surface topography rather than the full 3D volume scan of the object.

The application of XCT to micro-injection moulded products in a predictive quality assurance scheme or quality monitoring has not been reported in the literature to the authors' knowledge. One of the early reports investigated the feasibility of XCT for dimensional metrology of micro-injection moulded parts [25]. Their results concluded that XCT can be used for filling control and morphological characterisation of micromolded products with 8 and 15 μm voxel sizes. However, no scanning or exposure time data were presented in the work. XCT was effectively used for quantification of pore volumes up to 0.4 mm^3 in a V-shaped product mimicking typical medical device features. A total scan time of 60 min was reported, and total volume of the product was not disclosed [14]. Fibre volume content was also quantified using XCT for miniature polymeric test components, using scanning times of 150 and 190 min where overestimations based on voxel sizes were quantified [26]. The authors reported an overestimation of 300% in fibre volume for a voxel size of 8 μm in a simulation environment of 13 μm diameter glass fibres, which signifies the importance of acquisition parameter adjustment with respect to the feature size. These findings demonstrate XCT's excellent capability for quality assurance of micro-injection moulded components, however, the data was not used in conjunction with other process monitoring technologies and in-line quality predictive models.

The current work presents the utilisation of XCT for micro-injection moulded parts in a data-rich context that can be presented as an alternative to an industry standard metrology technique, LSCM. This is demonstrated as XCT's capability to establish predictive quality monitoring models in conjunction with the process data generated during the manufacturing process using external sensing technologies. For achieving this, an additively manufactured soft-tool was designed for producing a micro-featured circular object in back-to-back μ-IM cycles. Critical dimensional features were defined and extracted from the moulded objects using XCT and LSCM for comparison. Measurements have been compared and validated against maximum surface temperature of the soft-tool after the ejection of the mouldings to use the data for quality prediction of the mouldings. Deformations occurring on the soft-tool were also quantified by both measurement techniques and compared. A 3D overlay method was specifically applied for XCT which provided significant advantages for visualisation of deformations. The work presented here can be a significant contribution to the literature for 3D visualisation of micro-featured components with XCT as a demonstration of the technology to micro-manufacturing, quality assurance and prototyping applications.

2. Test object design and manufacture

2.1. Moulding object design

A circular test object containing microfeatures (Fig. 1a) was designed for manufacturing of the parts using μ-IM. It was used for comparative measurements on mould filling and quality assessment using XCT and LSCM. The dimensional details of the test object are given in Fig. 1b. The object design had 3 pairs of 6 mm wide micro-channels and micro-protrusions with a pyramidal profile and 0.6 mm depth or height. Each pair were separated by 3.5 mm. The upper end of the product had 0.8 mm diameter, 0.6 mm deep cylinder-shaped protrusion. Being at the far end of the product, this feature was designed to act as a filling indicator, and for making the moulding process more variation susceptible. These features also mimic typical dimensions that are being used for medical devices such as organ-on-chip, microfluidic devices, or connectors [27,28]. All of the microfeatures were oriented symmetrically onto a 13 mm diameter and 1.25 mm thick circular base. 3D CAD software (Solidworks, Dassault Systèmes, France) was used to generate the model and a negative version of the cavity was created onto a 55 mm diameter, 10.4 mm thick mould insert. A fan-type gate with 5 mm width and 1 mm depth was designed. A blank counterpart of the object was symmetrically placed on the mould insert for making the ejection process easier during de-moulding. The insert with the test object's negative impression cavity was fabricated using a J750 material jetting prototyping machine (Stratasys Ltd, USA) and fixed onto a bolster mould (Fig. 1c). The build was made in 'high-quality' and 'glossy finish' settings with a 14 μm layer thickness in the z-axis. The reason for the selection of soft-tooling method is to introduce additional variability in the process such as tool deformation as a disturbance to the process, so that it can be determined whether XCT can capture these variations.

2.2. Materials

A white, translucent resin (Vero PureWhite - RGD837, Stratasys Ltd, USA) was used in the J750 to additively manufacture the soft-tool. The soft-tool material was expected to be deformable in a cycle-by-cycle moulding process as it has a relatively low glass transition and heat deflection temperature compared to typical injection moulding conditions. This was thought likely to induce variations in each of the moulded prototype for XCT to detect changes throughout the process. The physical properties of the soft-tool material are given in Table 1.

Table 1
Physical properties of Vero PureWhite -RGD837 manufactured by Stratasys.

Properties	Value & units
Tensile strength	40 – 55 MPa
Modulus of elasticity	2200 – 3000 MPa
Heat deflection temperature	45–50 °C
Glass transition temperature	52 – 54 °C
Polymerised density	1.17 – 1.18 g/cm^3

2.3. Micro-injection moulding

Test objects were manufactured using the aforementioned mould combination on a μ-IM machine (Microsystems 50, Wittmann – Battenfeld UK, UK) (Fig. 2a). The moulding material was a widely used polypropylene (PP) resin (C711-70RNA, Braskem Europe, Germany). The process was optimised to run in fully-automatic mode, where the parts were ejected from the soft-tool using an automated ejector after each moulding cycle. The moulded test objects were collected from each cycle from the 1st to the 10th cycle, and then every 10th sample until the 100th, making 19 samples in total to be dimensionally characterised for the experiment. For each of the test objects, a maximum mould surface temperature (T_{max}) was also recorded inline using a thermal camera (Xi 410, Optris GmbH, Germany) (Fig. 2b) that offered a resolution of 384 × 240 pixels, a spectral range of 8–14 μm and a measuring accuracy of ± 2 °C. Cavity surface temperatures are known to represent the filling events in μ-IM processes [24,29,30]. Hence, T_{max} values were used to validate XCT data against LSCM for cavity filling and micro-feature replication that could be beneficial for in-line quality assurance and process modelling (Fig. 2c).

3. 3D visualisation methods

3.1. X-ray computerised tomography (XCT)

A Unitom XL micro XCT scanner (Tescan Orsay Holding, as, Czech Republic) was used for 3D visualisation of all 19 PP test objects. This particular XCT equipment combines a high-power X-ray source, fast frame rate detectors and efficient binning methods for high-temporal resolution which results in significantly reduced exposure and total acquisition times. The scanning parameters used for each of the mouldings are given in Table 2. The settings were chosen to provide a compromise between spatial resolution, noise reduction, and acquisition time, using a voxel size

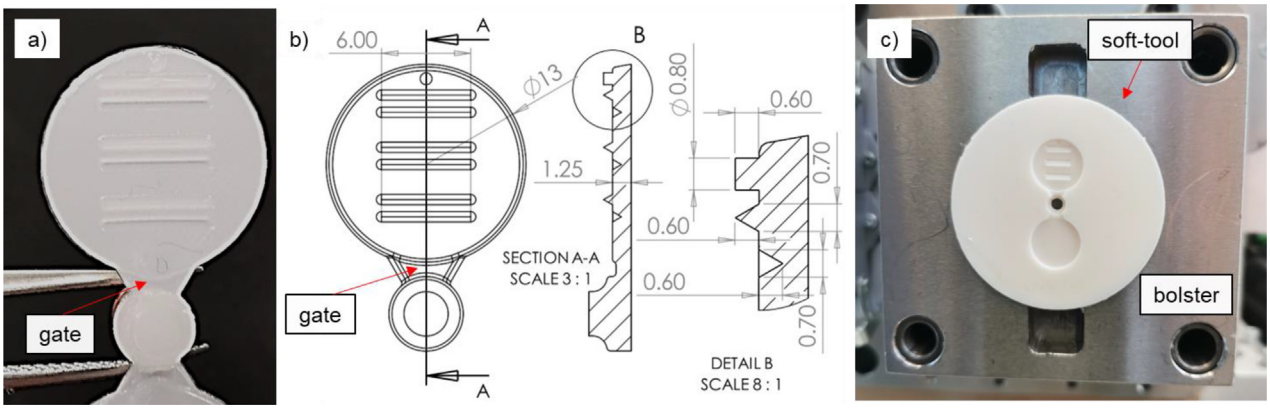

Fig. 1. Details of the test object design: a) an optical image showing the test object; b) dimensional details of the test object (dimensions in mm); c) soft-tool placed on the bolster mould.

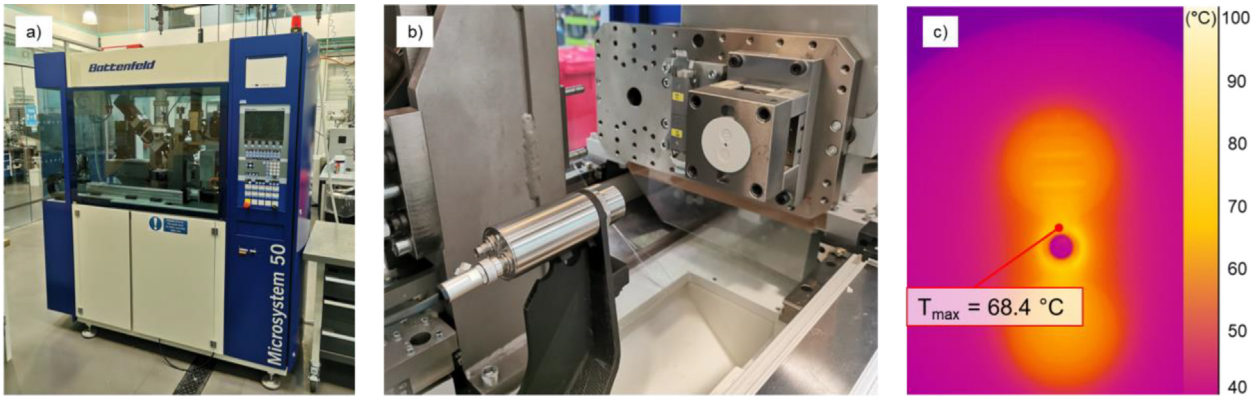

Fig. 2. Images depicting the manufacturing environment and process monitoring approach: a) Battenfeld Microsystem 50 micro-injection moulding machine; b) thermal camera attachment for soft-tool surface temperature measurements; c) a thermal image of the soft-tool showing the maximum temperature (68.4 °C) after ejection.

Table 2
Scanning parameters and information used in the XCT experiments for mouldings.

Parameter	Value & units
Exposure voltage	80 kV
Exposure power	15 W
Exposure time	81 ms
Voxel size	10 μm
# of projections	2279

of 10 μm to provide a sufficient resolution of all structures on the test part. The number of projections was defined by the Tuy-Smith criterion [31], using a cropped detector to reduce acquisition time at no expense of image quality. A Step-and-Shoot acquisition method was used to further reduce noise at the expense of scan time, where the stage stops between radiograph acquisitions rather than moving continuously.

XCT datasets were reconstructed using the standard FDK (Feldkamp, Davis and Kress) algorithm without a beam hardening correction due to the relatively low density of the PP test objects [4]. The post-processing and analysis of the XCT data was carried out in VGStudio Max 2.2 (Volume Graphics GmbH, Germany) and Avizo 2021.2 (Thermo Fischer Scientific, USA). In order to minimise spatial uncertainty, a voxel scaling process was used to calibrate the voxel size to a physical artefact [32]. To do this, a physical calibrated artefact was scanned before and after each disc sample was scanned at the same settings (see Table 3). The distance between the 3 spheres was measured in VG Studio Max 2.2 following segmentation using a standard ISO 50 algorithm and compared to the calibrated measurements. The deviation between these three measurements was used to calculate a scaling factor for each, which were then averaged together to create a single global scaling factor. This was then applied to the base voxel size to produce an adjusted voxel size of 10.00698 μm to be used for all subsequent volumetric data analysis.

3.2. Laser-scanning confocal microscopy (LSCM)

A LSCM (LEXT – OLS5000, Olympus - EVIDENT Europe GmbH, Germany) was used to perform surface scans of the test objects for the validation and comparison with XCT data. The microscope used a 405 nm light source for capturing the 3D topography of the surface by means of laser scanning. A 10x objective lens was used for acquiring surface point cloud data of the PP test objects using the stitching option. This resulted in a 3D acquisition of the micro-features on a 7 × 10.5 mm area on the surface of the sample. LSCM acquisition parameters are summarised in Table 4.

A visual representation of the XCT and LSCM data is given in Fig. 3. Fig. 3a shows an example of the reconstructed XCT data on a sample. The LSCM counterpart of the data is shown in Fig. 3b. 2D representation of the surface data shows LSCM's limitation in the total area acquisition which prevents a volumetric analysis of the whole part. However, the technique is known to capture the microfeatures with superior detail with 200 nm lateral and 100 nm vertical resolutions at 10x magnification [33]. It can also be seen from the figure that the features are rounded at the sharp edges due to the nature of the material jetting technique [34].

4. Results and discussion

4.1. Measurement and comparison method

Common measurands for XCT and LSCM were selected which allowed the comparison of measurements on the objects. Measurands were chosen for extraction in the same or most similar fashion for both techniques since the post processing of data vary depending on the software. Hence, the dome and ridge feature towards the far end of the product away from the gate has been selected to be analysed in detail as they are known to be more sensitive to pressure drops in the moulding processes (Fig. 3a and b) [19,35].

Table 3
Parameters for voxel scaling process.

Calibrated value (μm)	Value before scan (μm)	Deviation (%)	Value after scan (μm)	Deviation in percent	Voxel size scaled (μm)
8.3043	8.3069	1.000854979	8.3114	1.00054718	10.000698

Table 4
Parameters and conditions used in the LSCM acquisitions for test objects.

Parameter	Value & units
Objective lens	10x
Mode	Standard
Brightness	75.4%
Laser intensity	100%
Acquisition area (stitched)	4491 × 6687 pixels or 7 × 10.5 mm^2

The measurements have been classified in 2 different categories, namely: dimensional and volumetric measurements. Fig. 4 shows examples for profilometric and volumetric measurements that were extracted from 3D data for XCT and LSCM. The data processing and extraction were carried out in Avizo 3D 2021.2 (Thermo Fischer Scientific, USA) and Matlab R2020b (Mathworks, USA) software environments for XCT. As for LSCM data, OLS4100 software (3.1.15, Olympus - EVIDENT Europe GmbH, Germany) was used. The profiles in Fig. 4a show typical noise effects for LSCM when steep features are considered, particularly for the dome measurements. XCT's limitations in resolving capability of features in the z-axis can also be seen in the ridge acquisition where steps in the data are observed, which is a product of the voxelised nature of XCT data.

Height measurements included the height of the dome feature (H_D) and the lowest height point of the ridge features (L_R) as shown in Fig. 4a. The calculation of volumetric features for the dome and ridge given in Fig. 4b had to be performed in separate software due to data compatibility. Similar to the height measurements, volumetric measurements for the total volume of dome and ridge features (V_D and V_R) were calculated. One of the biggest advantages of using XCT in this study is the capability to calculate the total volume (V_T) of each of the micromoulded objects. LSCM had limited capability for calculating a total volume of the acquired point cloud, with a much smaller acquisition area (7 × 10.5 mm^2), that results in a much less representative measurement for part quality. Nevertheless, a total volume calculation was also performed for the LSCM data, where an upper plane above the top point of the microfeatures was selected.

It can be observed from Fig. 4a that XCT data captured the overall shape of both features with approximately 10 μm voxel size, yet some pixelations were seen while capturing flatter areas of the ridge feature that could bring shortcomings in terms of accuracy (see sub graph in Fig. 4a). Unfiltered LSCM data with blue curves

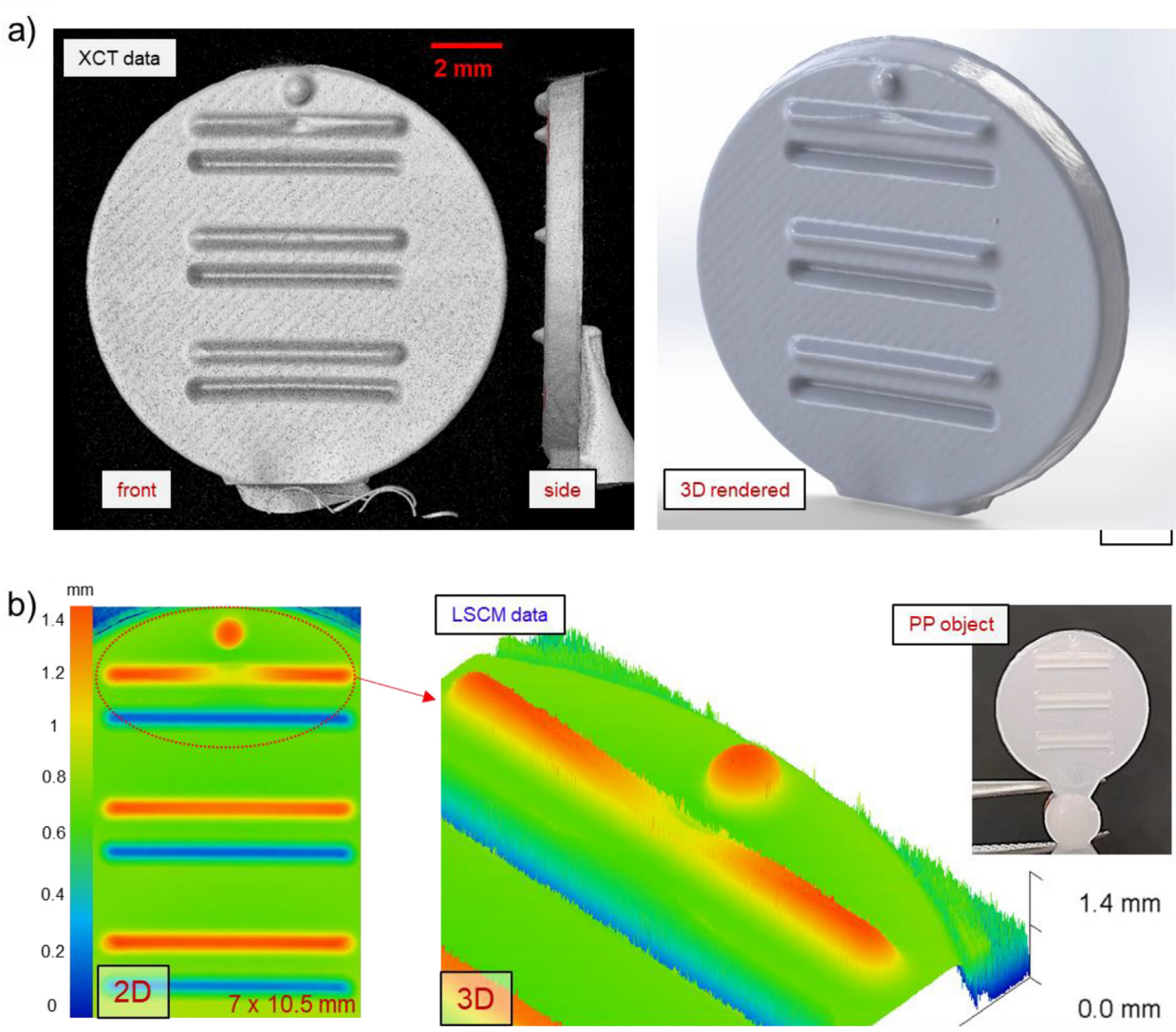

Fig. 3. 3D visualisation of the test objects: a) XCT data showing the 2D and 3D rendered images after reconstruction; b) LSCM data showing 2D and 3D representation of microfeatures on the test object.

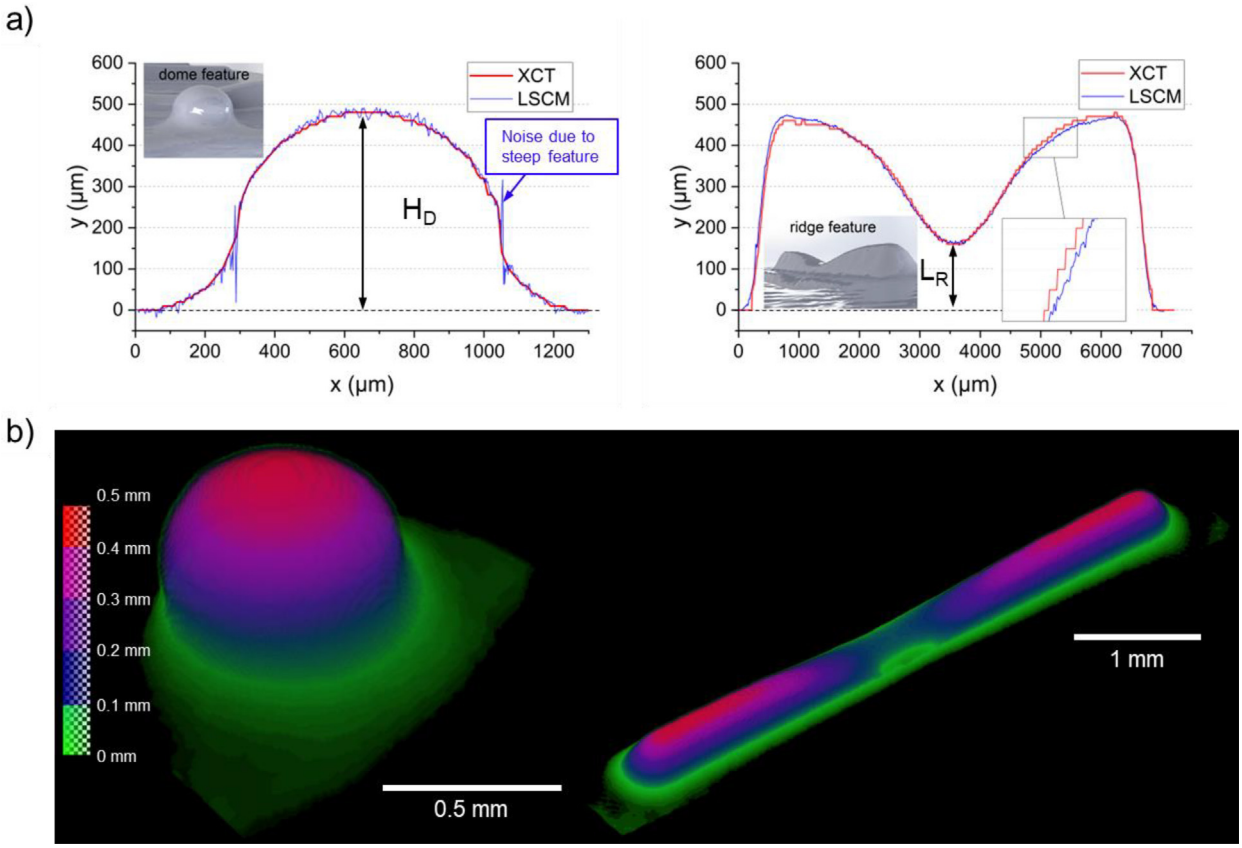

Fig. 4. Measurement examples from XCT and LSCM: a) data showing profiles for dome and ridge features including XCT and LSCM acquisitions; b) isolated dome and ridge features taken from XCT data.

also indicate that the steep features are challenging to capture, with inconsistent data peaks due to noise. From this perspective, although with limited feature detection capability, XCT can be a powerful tool for capturing micro-features with steep angles, without any optical restriction. Examples are presented in Fig. 4b from XCT data on how the final volume calculations were carried out for dome and ridge features based on the method given in the Appendix.

A repeatability test was carried out to quantify the variations that could occur due to the measurement algorithm or user judgment during post processing for both techniques. The first micro-moulded object was selected and each of the selected measurands were calculated 10 times to provide information regarding the repeatability of the measurement. Table 5 summarises the measurands and their statistical features, namely, mean and coefficient of variation (CoV) acquired from both techniques using XCT and LSCM (letters used in the abbreviations in Table 5). The results show that the measurement strategy for all measurands and both techniques provided satisfactory repeatability, where the highest CoV was found to be 3.9 % for volumetric ridge measurements with LSCM, $V_{R\text{-}LSCM}$.

The CoV data for height measurements (H_D and L_R) demonstrate LSCM's superior resolving capability vs XCT. Relatively higher CoV values for L_R and V_R values are seen due to the 3D aspect and plane selection procedures for both techniques. XCT presented better repeatability in all aspects for volumetric measurements, especially in the total volume with a CoV of only 0.5 % for $V_{T\text{-}XCT}$. This shows the significance of the 3D data acquisition of the object's volume as a whole, and the measurement variability mostly comes from the de-gating and cutting of the sample from the whole moulding volume.

4.2. Comparison of XCT data with LSCM

Each of the measurands given in Table 5 were calculated for all 19 mouldings. The measurements were analysed collectively against a real process measurement (T_{max}). The analysis and comparison included the following:

(1) Relative errors in % have been calculated for each measurand and object and then averaged (Table 6). The calculation was performed according to the formula below:

Table 5
An overview of the measurands used in the work and repeatability data acquired from the 1st sample.

Type	Measurand / feature	XCT Abbreviation	Mean (μm)	CoV (%)	LSCM Abbreviation	Mean (μm)	CoV (%)
Dimensional	Dome height (H_D)	$H_{D\text{-}XCT}$	481.6	1.19	$H_{D\text{-}LSCM}$	483.1	0.55
	Lowest ridge height (L_D)	$L_{R\text{-}XCT}$	160.9	4.17	$L_{R\text{-}LSCM}$	166.0	2.94
Volumetric	Dome volume (V_D)	$V_{D\text{-}XCT}$	0.210	2.18	$V_{D\text{-}LSCM}$	0.194	3.29
	Ridge Volume (V_R)	$V_{R\text{-}XCT}$	1.027	3.14	$V_{R\text{-}LSCM}$	1.068	3.90
	Total acquisition volume (V_T)	$V_{T\text{-}XCT}$	157.96	0.50	$V_{T\text{-}LSCM}$	42.19	1.99

Table 6
Relative errors between XCT and LSCM measurements. The data for total acquisition volume is n/a due to limited acquisition area of the LSCM measurement.

Type	Measurand / feature	Relative error (%)
Height	Dome height	2.16
	Lowest ridge height	20.48
Volumetric	Dome volume	3.98
	Ridge Volume	2.30
	Total acquisition volume	n/a

$$\varepsilon = \left|\frac{\vartheta_o - \vartheta_e}{\vartheta_e}\right| x100 \quad (1)$$

where, ε is the relative error, ϑ_o is the observed value and ϑ_e is the expected value. LSCM values were taken as the ϑ_e for benchmarking purposes.

(2) Scatter plots comparing XCT and LSCM data were generated. The trends and correlations between the two indicate the data extraction reliability for each of the techniques and the reliability of the selected measurand to be used as a "micro-manufacturing process fingerprint" [2,3]. Lower correlations between the two would mean that the chosen measurand is difficult to be quantified using the methods proposed in this work due to the deformations occurring in the soft-tool and process dynamics [17].

(3) Measurands were also analysed against the maximum surface temperature of the soft-tool after demoulding (T_{max}) which is indicative of the moulded object's degree of replication. Therefore, the correlations will inform to what degree XCT data can be used for quality quantification of micro-manufactured components, e.g., through process modelling using sensor data on comparison with LSCM.

Relative errors presented in Table 6 present XCT's limited capability in resolving single-point height measurements in z-axis, with a significant relative error in lowest ridge height measurements up to 20.48%. Height and volumetric measurements were grouped and analysed together based on the r-squared (r^2) values between XCT and LSCM measurements. Each technique was also benchmarked based on its correlation with respect to the process measurement (T_{max}) for comparison.

Scatter plots in Fig. 5 show the data for height measurements, namely $H_{D\text{-}XCT}$ and $H_{D\text{-}LS}$. The data in Fig. 5a indicate that the XCT measurements for dome height can represent LSCM measurements with excellent correlation with up to 97.7 % accuracy. However, the data points accumulating near 380 and 460 μm depict the same values for the x-axis which shows that XCT was not able to resolve the differences between these samples with its approximately 10 μm resolving capability in the z-axis. The strong correlations shown in Fig. 5b, and c show that the dome feature at the end of the cavity can be a good process or product quality indicator where the filling can be predicted up to circa 90% accuracy. The LSCM shows slightly better correlation than the XCT data because of its superior resolving capability in the z-direction for the dome feature. Similar comments can be made for the ridge feature measurements ($L_{R\text{-}XCT}$ and $L_{R\text{-}LSCM}$) where XCT data's inferior capability in resolving height resulted in multiple datapoints showing exactly the same values for XCT measurements. The lowest ridge height feature was found not to be relevant for prediction of the product quality over cycles, as the scattered behaviour of the data suggests in Fig. 5e and f indicates.

Volumetric data for dome and ridge features are given in Fig. 6. The comparison between the two techniques (Fig. 6a and d) does not show a significant correlation with up to only 79% accuracy. This is likely to be caused by the post processing of the data and limited flexibility in the LSCM data manipulation environment. The method for extracting the dome feature for XCT data proved to be marginally better as compared to the LSCM data (Fig. 6b and c). The inferior r^2 values depicted in Fig. 6e and f for micro-replication prediction of the parts are expected and justified where the bottom plane selection for the ridge feature has been particularly difficult for both techniques. Overall, XCT showed that it can definitely be used as a quality monitoring technique device for capturing micro-features in miniature products made out of

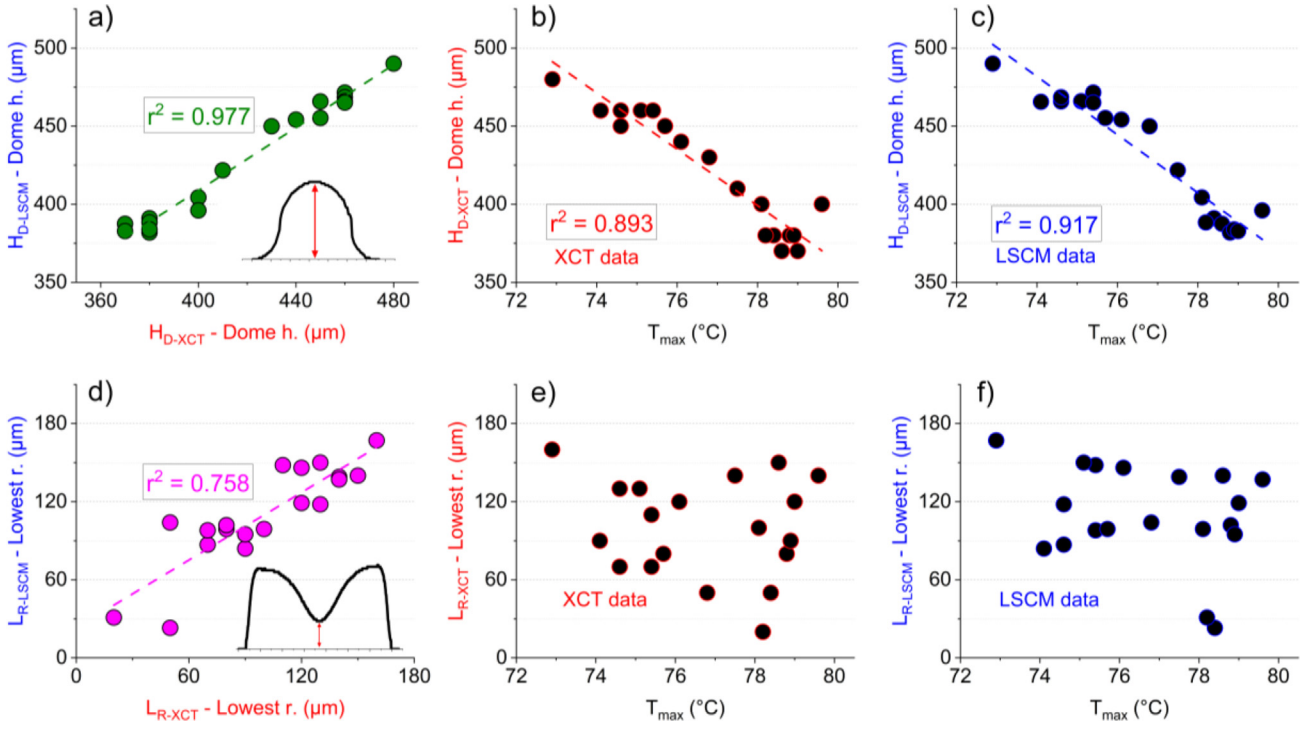

Fig. 5. XCT and LSCM height data in scatter plots; a) $H_{D\text{-}LSCM}$ vs $H_{D\text{-}XCT}$; b) $H_{D\text{-}XCT}$ vs T_{max}; c) $H_{D\text{-}LSCM}$ vs T_{max}; d) $L_{R\text{-}LSCM}$ vs $L_{R\text{-}XCT}$; e) $L_{R\text{-}XCT}$ vs T_{max}; f) $L_{R\text{-}LSCM}$ vs T_{max}.

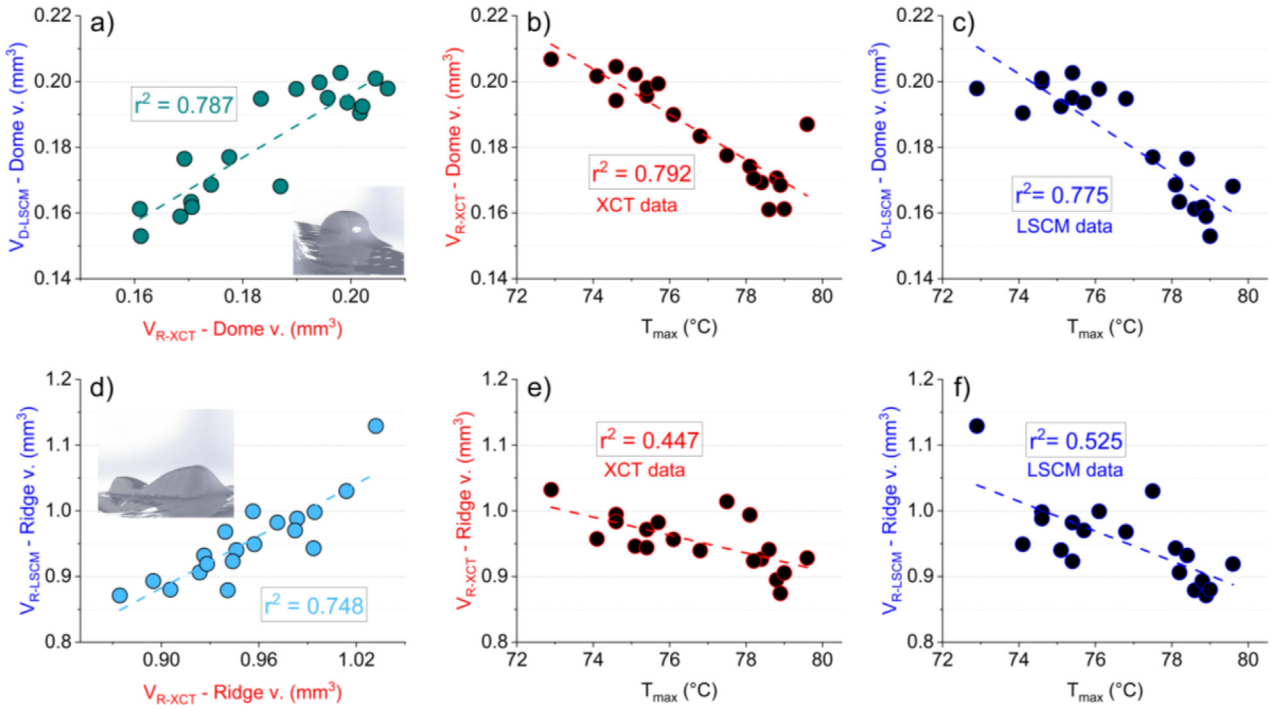

Fig. 6. Dome and ridge volume data for XCT and LSCM in scatter plots; a) $V_{D\text{-}LSCM}$ vs $V_{R\text{-}XCT}$; b) $V_{R\text{-}XCT}$ vs T_{max}; c) $V_{D\text{-}LSCM}$ vs T_{max}; d) $V_{R\text{-}LSCM}$ vs $V_{R\text{-}XCT}$; e) $V_{R\text{-}XCT}$ vs T_{max}; f) $V_{R\text{-}LSCM}$ vs T_{max}.

soft materials, up to with 89 % accuracy when collective measurements in a low or medium volume manufacture process are concerned.

The total volume acquisition from XCT and LSCM data is presented Fig. 7. The accuracy in predicting the filling quality of the test objects through collective XCT has been the particular highlight of this research with correlations reaching 92.1 % (Fig. 7b). This outperformed every other analysis made through XCT and LSCM data in this paper with its highest correlation with T_{max}. The result is significant since the volumetric XCT acquisition readily provides valuable information regarding the micro-manufacturing process quality without predefined quality indicators. It also implies that the reconstruction and voxelating steps can be automated and combined with XCT scanning for high-throughput applications. The total acquisition volume from LSCM ($V_{T\text{-}LSCM}$) on the other hand presented a scattered and random behaviour which was expected (Fig. 7c), due to the noise contributions around the scan of interest which could not be removed.

4.3. Indirect quantification of mould deformation using XCT data

Due to the thermal cycling during the moulding process, the soft-tools become deformed due to high temperatures, and adhesion forces occurring during ejection of the part from the mould [36]. In order to know to what extent the soft-tool deforms, it was essential to characterise the soft-tool before and after moulding of 100 test objects. Initially, LSCM was used to determine the final dimensions of the soft-tool and total volume of the cavity in which the objects were made by using the less accurate, however with faster 5x objective setting (scan time). Table 7 shows the LSCM volume measurement results for the pristine cavity and cavity volume after 100 cycles. The results show an overall 13 ± 0.2 % decrease in the volume due to soft-tool deformation after the moulding process.

Quantification of the mould deformation was performed using an indirect approach, where the XCT scans of the moulded objects were converted to standard triangle language (STL) files with mesh

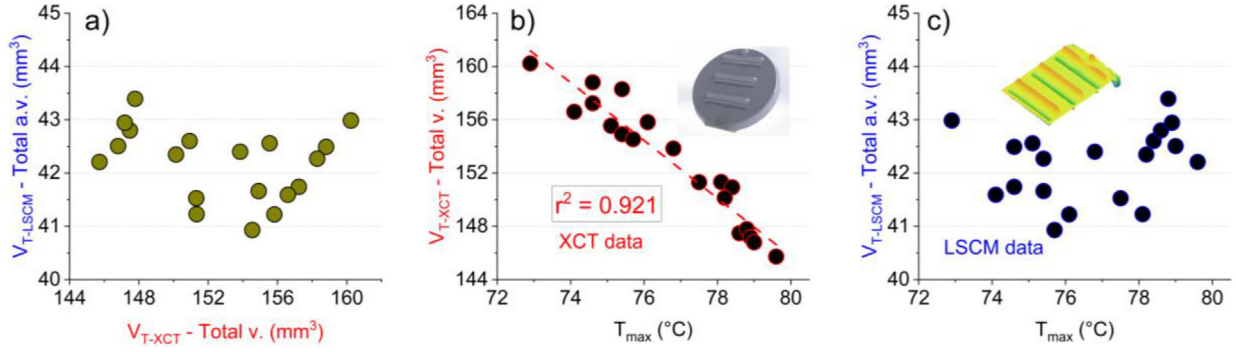

Fig. 7. Total volume acquisition data for XCT and LSCM in scatter plots; a) $V_{T\text{-}LSCM}$ vs $V_{T\text{-}XCT}$; b) $V_{T\text{-}XCT}$ vs T_{max}; c) $V_{T\text{-}LSCM}$ vs T_{max}.

Table 7
Parameters and conditions used in the LSCM acquisitions for test objects.

Pristine cavity volume (LSCM data)	Cavity volume after 100 cycles (LSCM data)
177 ± 1 mm^3	154 ± 1 mm^3

cleaning and then 3D overlays were carried out. The overlay procedure was performed using PolyWorks Metrology Suite: Inspector 2021 (InnovMetric Software Inc., Canada) using their built-in standard best-fit method. The software iteratively moves the floating dataset until a best-fit match between the two is achieved. A colourmap then can be output highlighting regions of deviation between the two samples. The overlays were done in a way that they were compared relative to each other, where each 10th sample was overlaid with the 1st sample (from the pristine cavity), which is considered as the "golden sample" with no or minimal deformation. Mappings were created in a 250 μm fixed scale showing the deviations above and below the ideal geometry.

Fig. 8 shows a comparison between two extreme overlay cases, namely 1st −10th and 1st – 100th for visualising the deviations. Both overlays show that moulded features deform below the nominal dimensions (smaller than nominal), predominantly on the areas closer to the gate and the centre of the objects. This is due to the higher temperatures of the melt and adhesion forces mainly accumulating near the centre of the parts. This results in a soft-tool deformation "above" the nominal, which results in the cavity volume decrease as indicated with dark blue regions in the 1st vs 100th comparison. The scales show a deformation in the range of 120 – 150 μm in the whole gate region for 100th part, which contributes to the main decrease in the cavity volume. Another highlight of the data given in Fig. 8 is that the XCT and overlay technique captured 3D visualisation of deviations at the micron scales as can be seen from the dome feature at the upper end of the cavity.

Overlays shown in Fig. 9 depicts the deformation on the soft-tool progressively from the 10th to the 100th cycles with mean deviation values for each overlay. It can be seen that between some cycle intervals, e.g. 20th – 30th and 40th – 50th, severe deformations mapped with dark blue and purple colours particularly near the gates somewhat tend to recover. The reasons for this are likely due to the complex thermomechanical behaviour and critical temperatures of the soft-tool used and it is not the focus of the current work. From the 10th to 100th moulding object, the deviations become significantly pronounced near the gate and middle sections of the cavity. The overall accumulation of deformations shown in blue, occurring in the central section of the part is once again due to higher temperatures experienced due to the fountain flow effect, which results in higher temperatures in the centre during the flow of the polymer [29,37,38]. Likewise, the green & yellow mappings on the sides show that the parts are above the ideal value, meaning that the tool is deforming towards the ejection direction in the centre, and in the opposite direction on the sides. It is depicted in the images that deviations as low as ~ 10 μm can be detected easily using the XCT overlay method. This could be a significant aspect of the analysis since the micro products made from soft materials can be scanned under XCT and overlays can be done relatively quickly for providing a reliable quality assurance method through design of experiments.

Scatter plots generated in Fig. 10 demonstrate the trends in filling of the moulding objects and deviations calculated from the overlay method. The y-axis in Fig. 10a represents the total volume calculated using XCT ($V_{T\text{-}XCT}$), however it has been normalised with the pristine cavity volume (172 mm^3) to show the % of the intended volume. The data show progressive deformation, which is in correspondence with the overlays provided in Fig. 10. The quantitative mean deviation acquired from the overlay method also compared against the XCT scan volume in Fig. 10b and shows excellent correlation. This validates both volumetric and overlay methods against each other and depending on the application, qualitative or quantitative analysis can easily be made for miniature components.

The volume data provided for the pristine mould and after 100 moulding cycles in Table 7 shows a 13 ± 0.2 % change in the cav-

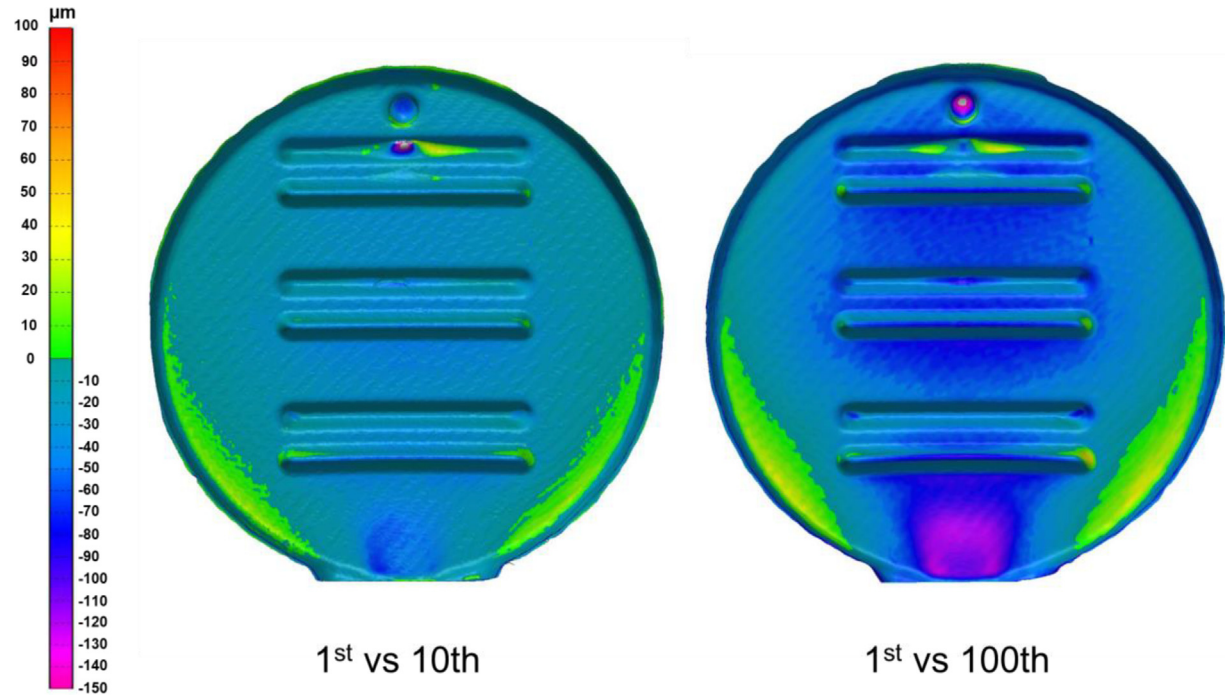

Fig. 8. Overlays and deviation mappings of XCT data of 10th and 100th sample in comparison to 1st.

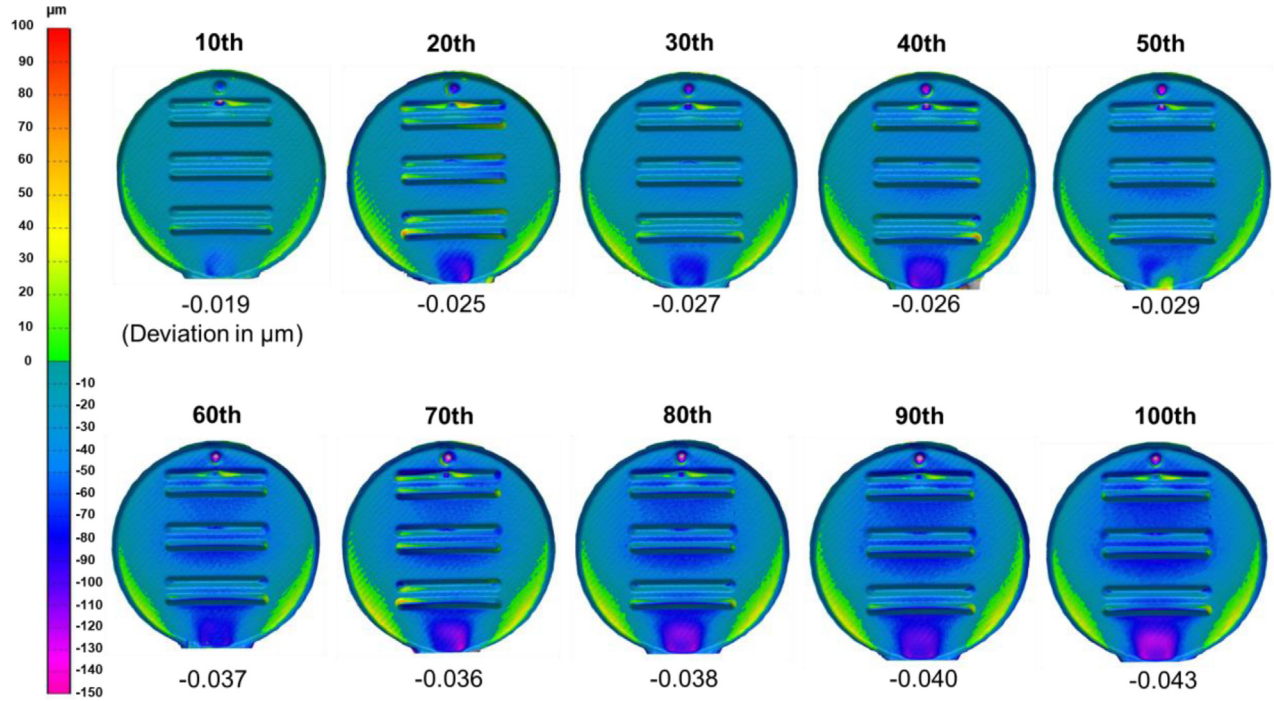

Fig. 9. Overlays and deviation mappings of XCT data of every 10th sample from the manufacturing runs. Mean deviation values for each overlay are shown beneath each colour map in µm.

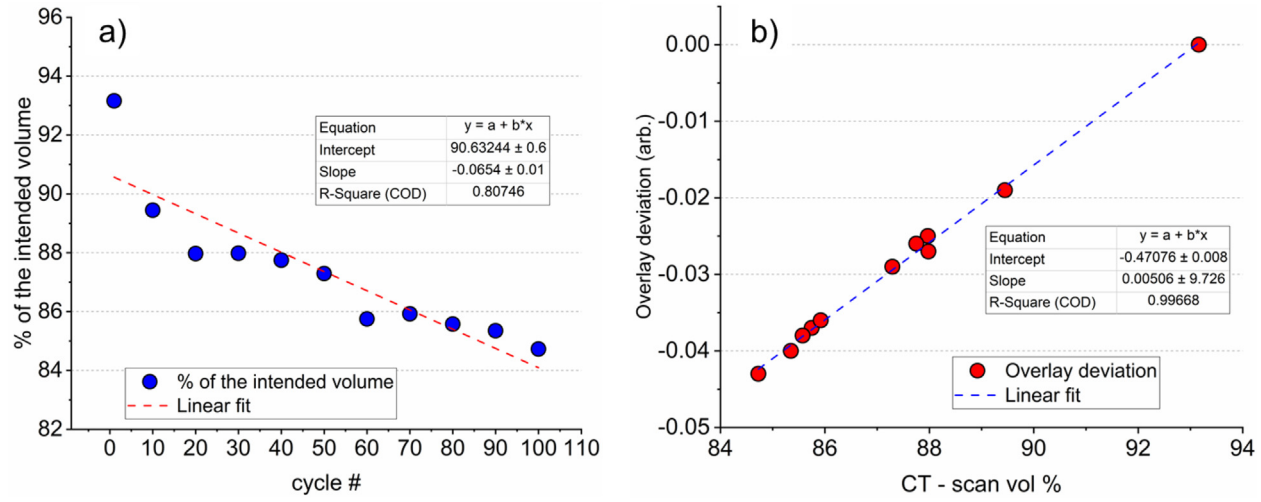

Fig. 10. XCT and overlay data showing: a) % filling of the intended volume over moulding cycles; b) scatter plot showing the relationship between overlay deviation and CT scan volume %.

ity/part volume. Calculation was carried out for determining to what extent this value can be quantified indirectly, through XCT data. Calculation was made based on the 1st and 100th moulding's XCT volumetric data as following.

$$\frac{(160.2 - 145.7)}{160.2} = 9.05\% \quad (2)$$

There is a significant difference in the cavity volume according to the above calculation and the data in Table 7. The reason for this is that the calculation using LSCM data given in Table 7 is not affected by shrinkage whereas the indirect measurement is. The shrinkage of PP as a semi-crystalline polymer is approximately 2% and is significant. Additionally, the short shot aspect of the experiment demonstrated in this work may have left some parts of the cavity unfilled. However, the dosing unit of the µ-IM machine is very accurate which was not expected to have an impact on this calculation [17,39]. It can be said that indirect soft-tool deformation through XCT data can be a good approximation. To summarise, provided that a full replication and industrial standard mould tool is used, the calculation also proved that volumetric changes in the moulding cavity can be approximated indirectly using XCT data.

4.4. Global comparison

This section compares XCT and LSCM in terms of key features such as acquisition time, height resolution and their potential

Table 8
XCT and LSCM global comparison based on key measurement features.

Feature	XCT	LSCM
Acquisition area/volume	Full volume & area acquisition of the micromoulded product	Topographical data from 7 × 10.5 mm^2 area corresponds to 64 mm^3 (only ~ 40 % of the total volume)
Internal volumetric inspection capability	Possible with full volume acquisition capability	Only surface topographical data collected, internal inspection not possible
Total scan time	18 mins	20 mins
The best correlating measurement for quality prediction	Total acquisition volume ($V_{T\text{-}XCT}$), 92.1%	Dome height ($H_{D\text{-}LSCM}$), 91.7%
Height resolution in z-axis	10 μm	0.1 μm

usage in quality predictive models for micro-manufacturing applications. These key features are summarised in Table 8.

Firstly, the measurement approach and selection of key dimensional features worked satisfactorily for both techniques where sufficient repeatability was achieved. Generally speaking, XCT will have limited resolving power in the measurement of step-height features for micro-scaled parts and LSCM performs significantly better with its 0.1 μm resolution in the z-axis. However, for volumetric capture of the 3D data for specific features on the microstructured product, XCT performed better in terms of the acquisition of repeatable measurements, even though challenges were present in base-plane selections due to the soft-tool deformation. XCT's superior performance over LSCM was very obvious when acquiring the whole 3D volume of the product with CoV approaching 0.5 %. This also required minimal post processing with no geometrical reference or base plane selections, and shows significant potential for quality inspection or prediction micro-injection moulded components [22].

XCT's excellent performance in capturing volumes and their correlation to the manufacturing process quality was also validated using process measurements (T_{max}), and the total volume acquisition correlated up to 92.1 % for prediction of the filling compared to inferior correlations obtained from dimensional measurements. LSCM was marginally superior from this perspective in height measurements where it reached 91.7% accuracy, compared to mostly scattered behaviour in volumetric measurements.

Total volumetric acquisition of micromoulded parts also proved to be very useful for qualitative & quantitative analysis when per-

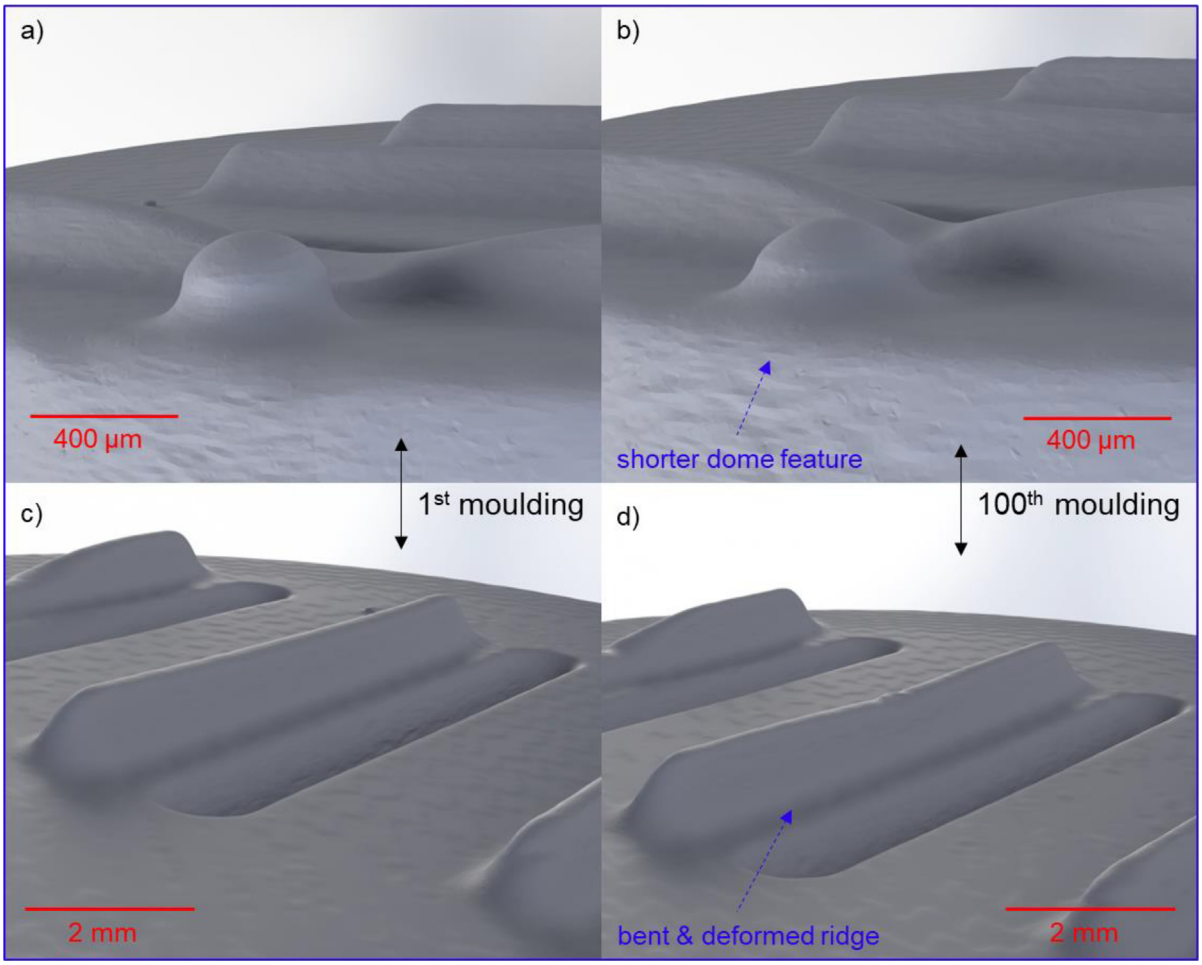

Fig. 11. Rendered images generated from STL data acquired from XCT scans: a-b) Close up of dome feature for the 1st and 100th sample, c-d) Close-up of middle ridge feature for the 1st and 100th sample.

forming STL overlays. Using this approach, although it is an indirect measurement, faults in the moulding cavities and products can be quantified easily and design of experiments can be carried out. The overlay mappings enable the visualisation of deviations in critical features down to 10 μm ranges.

In terms of data acquisition times, XCT is very competitive with 18 min required for capturing the full-3D data of the micro-moulded component. Similar scanning times are required for LSCM for an image stitching of only topographical data with a limited acquisition area, and this has been one of the highlights of this research for showing XCT's excellent capability. It should also be noted that there are multiple steps in reconstruction of the XCT data which could add to his acquisition time, however, the particular software and XCT suite combination showed great potential in customisation and automation especially for the whole 3D volume of the parts.

XCT also provides significant advantages in term of post-processing flexibility where the acquired point-clouds can be converted into 3D models and rendered images can be generated for demonstration purposes (Fig. 11). The close-up rendering of images was performed in Solidworks Visualise Professional (Dassault Systèmes, France) for detailed examination of the 1st and 100th mouldings. Fig. 11a and b show the obvious differences in the dome height feature. Ridge features were also visualised in close-up images where slightly bent middle section of the ridge was able to be detected. To summarise, the XCTs ability to capture 3D data can be an extremely powerful method to visually inspect miniature small polymeric components combined with advanced rendering solutions.

Following suggestions can be made for exploiting the potential of XCT in micro-manufacturing applications:

- Resolution can still be taken down towards 5 μm from 10 μm and this will result in a significant increase in quality correlations with process measurements resulting in more accurate and precise in-line quality assurance models. However, this will result in an increase in scan times and the need for XCT resource in terms of labour and equipment times.
- The quality predictive aspect of XCT can be utilised through design of experiments, where micro-injection moulding variations can be determined per process parameter (temperature, dosing, pressure etc.) and quality assessment of products can be automated.

In summary, aspect of XCT can become a very powerful method for quality control steps in micro-manufacturing if the scan parameters and post-processing are optimised as shown herein. LSCM still is, and will be, one of the state-of-the-art techniques for applications requiring resolutions down to the micro and nanoscale. The technique also provides minimal material limitations including reflection, transparency, or opaqueness of the measured sample. However, XCT's full 3D data acquisition capability show excellent potential for its usage in micro-manufacturing applications and for creation of in-line inspection models in conjunction with additional process monitoring devices.

5. Conclusions

In this research, we demonstrated the capability of XCT for the 3D characterisation of micro-injection moulded components and soft-tool deformation assessment for the first time in the literature. Scanning times of 18 min and a voxel size of 10 μm in the current study were found to be sufficient to demonstrate XCTs capability for the creation of quality prediction models for micro-injection moulding [14]. The results were compared and validated against a state-of-the-art LSCM. The particular highlight of this research is the XCT's capability in acquiring the whole 3D data of the product in relatively fast scans and its effectiveness in reaching and even surpassing a highly-capable microscopy technique in 3D visualisation and quality prediction. Representation of the XCT data was qualitatively and quantitatively made by comparing it against real process measurements and overlay methods for defect detection and quality control. Main highlights of this research can be summarised as following:

- Demonstration of a state-of-the-art XCT machine using soft-materials and its potential usage for high-added value, micro-injection moulded components and tool deformation,
- Exploitation of 3D data acquisition capability of XCT for quality predictive models in micro-manufacturing applications,
- Presentation of both quantitative and qualitative XCT data for the characterisations of miniature products through overlays and predictive analysis,
- Demonstration of XCT that it can perform or even surpass the performance of a common metrology device for dimensional characterisation of technological products when the right settings and measurement approaches are implemented.

Author contributions

Mert Gulcur wrote the manuscript, performed micro-injection moulding, laser-scanning confocal microscope experiments and analysed all the data. Paul Wilson performed XCT experiments, developed XCT data extraction method & coding and analysed data. Michael Donnelly carried out STL overlays and extracted deviation data. Kevin Couling and Vannessa Goodship contributed to micro-injection moulding experiments. Jerome Charmet, Mert Gulcur, Mark Williams, and Gregory Gibbons acquired funding. We thank Dr Guillaume Remy for providing the voxel scaling data. All authors have read and contributed to the writing & editing of the manuscript.

Data availability

Data will be made available on request.

Declaration of Competing Interest

The authors declare that they have no known competing financial interests or personal relationships that could have appeared to influence the work reported in this paper.

Acknowledgements

This research has been funded and supported by multiple sources. The X-Ray Computed Tomography (XCT) data used in this article was acquired using the Free-at-Point-of-Access scheme at the National Facility for X-Ray Computed Tomography (NXCT) and carried out at the Centre for Imaging, Metrology, and Additive Technologies (CiMAT) at the University of Warwick under the EPRSC Project Number (EP/T02593X/1 and EP/S010076/1). Soft-tooled micro-injection moulding process demonstrated in this work was funded by the High Value Manufacturing Catapult (HVMC) and was developed under the project "Capacity Building for Prototyping Compatible Injection Moulding (Project no: 8225)". Authors also would like to thank Mrs Jane Bratherton from Olympus - EVIDENT Europe GmbH for the arrangement of the in-kind laser-scanning confocal microscope trial period in our facilities and for collaborating with WMG.

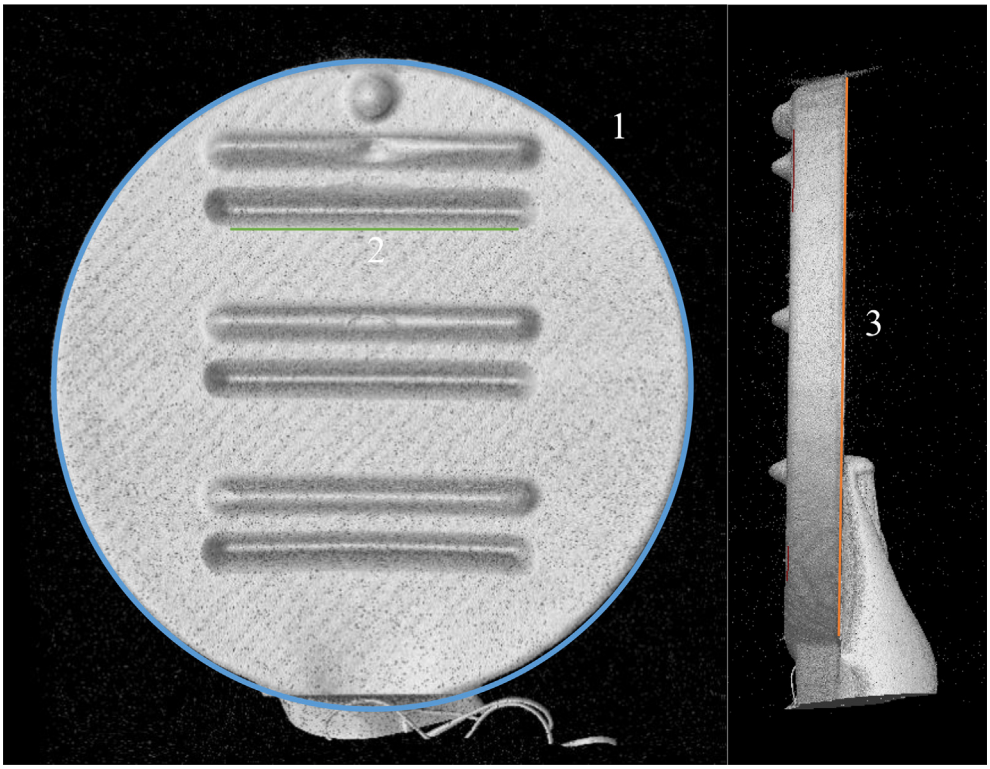

Fig. A1. Location of Common Structures used for Global Alignment of Samples.

Appendix A. XCT measurement method

Once the datasets had been imported into VGStudio Max 2.2 following the voxel scaling procedure (see 3.1 sigh-speed XCT), a surface determination was calculated using a standard ISO 50 algorithm. The samples were then aligned using three common features to all samples (see Figure A): 1) A circle defined around the perimeter of the back plane of the disc; 2) A line defined along the bottom edge of the first trough; 3) The back plane of the disc (see Fig. A1).

A 3-2-1 registration was then performed using these features, resulting in all of the analysed datasets having the same alignment system for better quality measurement. Once aligned, both the dome, ridge and total disc areas were extracted as Regions-of-Interest (ROIs). The base of these was defined by the lowest pixel of the feature. These datasets were then exported as.tiff stacks to be analysed in different software according to the needs of the measurements to be performed as follows:

- Total Volume of Disc (Avizo 3D 2021.2)
- Elevation profile of Ridge (YZ) and Dome (XY; YZ) (Matlab R2020b)
- Height Map of Ridge and Dome (Avizo 3D 2021.2)
- Volume of Ridge and Dome (Avizo 3D 2021.2)

In Avizo 3D 2021.2, an anisotropic diffusion filter was first used to reduce noise in all three volumes. Then, all three volumes were thresholded using the Otsu method and subjected to an opening/-closing operation with a 3px ball structuring element to reduce noise.

For the Total Volume of Disc, a label analysis was performed using the Volume3D parameter on the whole disc volume. The Extracted volume used was the whole disc, bounded by the first slice where the mount can be clearly defined and the base of Feature 1. For the Volume of Ridge and Dome, a label analysis was performed using the Volume3D parameter on the ridge and dome volume respectively. Images and height maps were produced by creating a label field defining the lowest slice in the dataset. Using this, a distance map was generated from this base. This field was then masked using the Mask function, using the Ridge or Dome dataset respectively to create a height map. This was then rendered in colour and images produced for both structures.

In Matlab R2020b, the datasets were loaded in and binarized using the Otsu method and subjected to an opening/closing operation using a 3px disc structuring element to reduce noise. The centroid of the feature (disc or ridge) was found using a representative slice and the central image in the stack extracted from both the dome and ridge structures. The first occurrence of the binarized structure from the top of this central image in all columns was then found, the distance scaled by the voxel size and then exported as.csv files for further analysis as a profile. This method was used in both the repeatability study and for the full analysis of all discs.

Appendix B. Supplementary data

Supplementary data to this article can be found online at https://doi.org/10.1016/j.matdes.2023.111741.

References

[1] E.B. Brousseau, S.S. Dimov, D.T. Pham, Some recent advances in multi-material micro- and nano-manufacturing, Int. J. Adv. Manuf. Technol. 47 (1) (2010/03/01 2010) 161–180, https://doi.org/10.1007/s00170-009-2214-5.
[2] F. Baruffi, M. Calaon, G. Tosello, "Micro-Injection Moulding In-Line Quality Assurance Based on Product and Process Fingerprints,", (in eng) Micromachines 9 (6) (2018) 293, https://doi.org/10.3390/mi9060293.
[3] M. Gülçür, B. Whiteside, A study of micromanufacturing process fingerprints in micro-injection moulding for machine learning and Industry 4.0 applications, Int. J. Adv. Manuf. Technol. 115 (5–6) (2021) 1943–1954, https://doi.org/10.1007/s00170-021-07252-7.
[4] L.A. Feldkamp, L.C. Davis, J.W. Kress, Practical cone-beam algorithm, J. Opt. Soc. Am. A 1 (6) (1984/06/01 1984) 612–619, https://doi.org/10.1364/JOSAA.1.000612.

[5] J.P. Kruth, M. Bartscher, S. Carmignato, R. Schmitt, L. De Chiffre, A. Weckenmann, Computed tomography for dimensional metrology, CIRP Ann. 60 (2) (2011/01/01/ 2011) 821–842, https://doi.org/10.1016/j.cirp.2011.05.006.
[6] E.A. Zwanenburg, M.A. Williams, J.M. Warnett, Review of high-speed imaging with lab-based x-ray computed tomography, Meas. Sci. Technol. 33 (1) (2022) 012003.
[7] A. Du Plessis, I. Yadroitsev, I. Yadroitsava, S.G. Le Roux, "X-Ray Microcomputed Tomography in Additive Manufacturing: A Review of the Current Technology and Applications,", 3D Printing and Additive Manufacturing Article 5 (3) (2018) 227–247, https://doi.org/10.1089/3dp.2018.0060.
[8] A. du Plessis, M. Tshibalanganda, S.G. le Roux, "Not all scans are equal: X-ray tomography image quality evaluation," *Materials Today*, Communications 22 (2020/03/01/ 2020), https://doi.org/10.1016/j.mtcomm.2019.100792 100792.
[9] W. Niu, H. Xiao, H. Ying, Y. Xu, Y. Zhang, "Micro-computed tomography to assess the processing quality of the additive manufacturing of spiral microcoils,", 3D Printing and Additive Manufacturing Article 7 (2) (2020) 70–77, https://doi.org/10.1089/3dp.2019.0114.
[10] W. Dewulf, H. Bosse, S. Carmignato, R. Leach, Advances in the metrological traceability and performance of X-ray computed tomography, CIRP Ann. 71 (2) (2022) 693–716.
[11] a. s. Tescan Orsay Holding. "Discover how resolution, speed, image quality and system versatility work together and provide the optimal micro-CT experience." https://www.tescan.com/discover-how-resolution-speed-image-quality-and-system-versatility-work-together-and-provide-the-optimal-micro-ctexperience/ (accessed 21.08.2022, 2022).
[12] J. Dewanckele, M.A. Boone, F. Coppens, D. van Loo, A.P. Merkle, Innovations in laboratory-based dynamic micro-CT to accelerate in situ research, J. Microsc. 277 (3) (2020) 197–209, https://doi.org/10.1111/jmi.12879.
[13] E.A. Zwanenburg, M.A. Williams, J.M. Warnett, Performance testing of dimensional X-ray computed tomography systems, Precis. Eng. 77 (2022/09/01/ 2022) 179–193, https://doi.org/10.1016/j.precisioneng.2022.05.005.
[14] J.S. Rathore, G. Lucchetta, S. Carmignato, Towards Optimization of μ-Injection Molding Process for a New V-Shaped Geometrical Component Using X-ray CT-Based Quality Characterization, Journal of Manufacturing and Materials Processing 3 (1) (2019), https://doi.org/10.3390/jmmp3010013.
[15] N. Kourra, J.M. Warnett, A. Attridge, G. Dibling, J. McLoughlin, S. Muirhead-Allwood, R. King, M.A. Williams, Computed tomography metrological examination of additive manufactured acetabular hip prosthesis cups, Addit. Manuf. 22 (2018) 146–152.
[16] M. Worgull, *Hot embossing: Theory and technology of microreplication* (Hot Embossing, Theory and Technology of Microreplication) (2009) 1–239.
[17] B.R. Whiteside, M.T. Martyn, P.D. Coates, G. Greenway, P. Allen, P. Hornsby, Micromoulding: Process measurements, product morphology and properties, Plast., Rubber Compos. 33 (2004) 11–17, https://doi.org/10.1179/146580104225018346.
[18] H.N. Hansen, K. Carneiro, H. Haitjema, L. De Chiffre, Dimensional micro and nano metrology, CIRP Ann. Manuf. Technol. 55 (2) (2006) 721–743, https://doi.org/10.1016/j.cirp.2006.10.005.
[19] M. Gülçür, J.-M. Romano, P. Penchev, T. Gough, E. Brown, S. Dimov, B. Whiteside, A cost-effective process chain for thermoplastic microneedle manufacture combining laser micro-machining and micro-injection moulding, CIRP J. Manuf. Sci. Technol. 32 (2021) 311–321.
[20] B.R. Whiteside, R. Spares, K. Howell, M.T. Martyn, P.D. Coates, Micromoulding: Extreme process monitoring and inline product assessment, Plast., Rubber Compos. 34 (9) (2005) 380–386, https://doi.org/10.1179/174328905X72011.
[21] D. Li, Y. Zhang, Y. Liu, F. Regi, M.E. Brix Doest, G. Tosello, Injection moulding of mechanical micro-manufactured structures for optically encoding plastic surfaces, Opt. Mater. 123 (2022/01/01/ 2022), https://doi.org/10.1016/j.optmat.2021.111822 111822.
[22] G. Tosello, "Product/process fingerprint in micro manufacturing," *Micromachines,* vol. 10, no. 5, 2019, Art no. 340, doi: 10.3390/mi10050340.
[23] T. Santoso, W.P. Syam, S. Darukumalli, R. Leach, Development of a compact focus variation microscopy sensor for on-machine surface topography measurement, Measurement 187 (2022) 110311.
[24] F. Baruffi, M. Gülçür, M. Calaon, J.-M. Romano, P. Penchev, S. Dimov, B. Whiteside, G. Tosello, Correlating nano-scale surface replication accuracy and cavity temperature in micro-injection moulding using in-line process control and high-speed thermal imaging, J. Manuf. Process. 47 (2019) 367–381.
[25] S. Ontiveros, J.A. Yagüe-Fabra, R. Jiménez, G. Tosello, S. Gasparin, A. Pierobon, S. Carmignato, H.N. Hansen, Dimensional measurement of micro-moulded parts by computed tomography, Meas. Sci. Technol. 23 (12) (2012) 125401.
[26] J.S. Rathore, T. Konopczyński, J. Hesser, G. Lucchetta, S. Carmignato, Investigation on Tomographic-Based Nondestructive Characterization of Short Glass Fiber-Reinforced Composites as Obtained From Micro Injection Molding, Journal of Nondestructive Evaluation, Diagnostics and Prognostics of Engineering Systems 3 (2) (2020) pp, https://doi.org/10.1115/1.4046000.
[27] B. Camli, O.K. Erden, O.F. Sezgen, Z.C. Canbek Ozdil, S. Dumanli, A.E. Pusane, A. D. Yalcinkaya, T. Tugcu, Rapid prototyping of noncontact microwave microfluidic devices for sensing applications, J. Micromech. Microeng. 31 (9) (2021) 097001.
[28] A.B. Sözmen, A. Arslan Yildiz, Cost-effective and rapid prototyping of PMMA microfluidic device via polymer-assisted bonding, Microfluid. Nanofluid. 25 (8) (2021/07/05 2021) 66, https://doi.org/10.1007/s10404-021-02466-3.
[29] M. Babenko, J. Sweeney, P. Petkov, F. Lacan, S. Bigot, B. Whiteside, Evaluation of heat transfer at the cavity-polymer interface in microinjection moulding based on experimental and simulation study, *Appl. Therm. Eng.* Article 130 (2018) 865–876, https://doi.org/10.1016/j.applthermaleng.2017.11.022.
[30] M. Gülçür, E. Brown, T. Gough, J.-M. Romano, P. Penchev, S. Dimov, B. Whiteside, Ultrasonic micromoulding: Process characterisation using extensive in-line monitoring for micro-scaled products, J. Manuf. Process. 58 (2020) 289–301.
[31] B.D. Smith, Image Reconstruction from Cone-Beam Projections: Necessary and Sufficient Conditions and Reconstruction Methods, IEEE Trans. Med. Imaging 4 (1) (1985) 14–25, https://doi.org/10.1109/TMI.1985.4307689.
[32] J. Lifton and J. McBride, *The application of voxel size correction in X-ray computed tomography for dimensional metrology*. 2013.
[33] Olympus. "LEXT™ OLS5100 3D Laser Scanning Microscope." https://www.olympus-ims.com/en/microscopes/laser-confocal/ols5100/ (accessed 08.09.2022, 2022).
[34] H. Yang, J.C. Lim, Y. Liu, X. Qi, Y.L. Yap, V. Dikshit, W.Y. Yeong, J. Wei, Performance evaluation of ProJet multi-material jetting 3D printer, Virtual and Physical Prototyping 12 (1) (2017) 95–103.
[35] H.-Y. Zhang, N. Zhang, W. Han, H.-G. Zhang, M.D. Gilchrist, F.-Z. Fang, Characterization of process and machine dynamics on the precision replication of microlens arrays using microinjection moulding, Advances in Manufacturing 9 (3) (2021/09/01 2021) 319–341, https://doi.org/10.1007/s40436-020-00341-y.
[36] C. A. Griffiths, S. S. Dimov, S. G. Scholz, G. Tosello, and A. Rees, "Influence of injection and cavity pressure on the demoulding force in micro-injection moulding," *Journal of Manufacturing Science and Engineering, Transactions of the ASME,* vol. 136, no. 3, 2014, Art no. 031014, doi: 10.1115/1.4026983.
[37] C.A. Griffiths, S.S. Dimov, E.B. Brousseau, R.T. Hoyle, The effects of tool surface quality in micro-injection moulding, J. Mater. Process. Technol. 189 (1) (2007/07/06/ 2007) 418–427, https://doi.org/10.1016/j.jmatprotec.2007.02.022.
[38] D. Masato, M. Sorgato, M. Babenko, B. Whiteside, G. Lucchetta, Thin-wall injection molding of polystyrene parts with coated and uncoated cavities, *Mater. Des.* Article 141 (2018) 286–295, https://doi.org/10.1016/j.matdes.2017.12.048.
[39] B.R. Whiteside, M.T. Martyn, P.D. Coates, P.S. Allan, P.R. Hornsby, G. Greenway, Micromoulding: Process characteristics and product properties, Plast., Rubber Compos. 32 (6) (2003) 231–239, https://doi.org/10.1179/146580103225002650.